Wind and Structures, *Vol. 17, No. 5 (2013) 515-535*
DOI:http://dx.doi.org/10.12989/was.2013.17.5.515

Experimental and numerical studies of the flow around the Ahmed body

Tural Tunay, Besir Sahin* and Huseyin Akilli

Department of Mechanical Engineering, Cukurova University, 01330, Adana, Turkey

(Received September 24, 2012, Revised April 21, 2013, Accepted July 11, 2013)

Abstract. The present study aims to investigate characteristics of the flow structures around the Ahmed body by using both experimental and numerical methods. Therefore, ¼ scale Ahmed body having 25° slant angle was employed. The Reynolds number based on the body height, H and the free stream velocity, U was Re_H=1.48x10^4. Investigations were conducted in two parts. In the first part of the study, Large Eddy Simulation (LES) method was used to resolve the flow structures around the Ahmed body, numerically. In the second part of the study the particle image velocimetry (PIV) technique was used to measure instantaneous velocity fields around the Ahmed body. Time-averaged and instantaneous velocity vectors maps, streamline topology and vorticity contours of the flow fields were presented and discussed in details. Comparison of the mean and turbulent quantities of the LES results and the PIV results with the results of Lienhart *et al.* (2000) at different locations over the slanted surface and in the wake region of the Ahmed body were also given. Flow features such as critical points and recirculation zones in the wake region downstream of the Ahmed body were well captured. The spectra of numerically and experimentally obtained stream-wise and vertical velocity fluctuations were presented and they show good consistency with the numerical result of Minguez *et al*. (2008).

Keywords: Ahmed body; bluff body; flow separation; LES; PIV

1. Introduction

Ground vehicles, in view of Fluid Mechanics, can be thought as bluff bodies which move very close proximity to the ground. The flow around the ground vehicles is fully three-dimensional and turbulent (Hucho and Sovran 1993). Bluff bodies are characterised by flow separations from their surface, wakes and unsteady velocity fields. Locations of the flow separation downstream of the bluff bodies are forced by their geometry and do not change considerably with both Reynolds number and upstream flow conditions. There are considerable studies on the ground vehicles and bluff bodies in close proximity to the ground in the previous literature (Ahmed *et al.* 1984, Cooper 1985, Barlow *et al*. 1999, Krajnovic and Davidson 2003, Gurlek *et al*. 2008, Sharma *et al*. 2008).

Flow around the Ahmed body is similar to the flow around prismatic bluff bodies. Ahmed body is a semi-rectangular vehicle shape with a rounded front part and a slant back which retains some main features of the flow around real cars and generates fully three-dimensional regions of

*Corresponding author, Professor, E-mail: bsahin@cu.edu.tr

http://www.techno-press.org/?journal=was&subpage=8 ISSN: 1226-6116 (Print), 1598-6225 (Online)

separated flow (Guilmineau 2008). It was first employed by Ahmed *et al.* (1984) and since then it has been used in several experimental (Lienhart *et al.* 2000, Spohn and Gillieron 2002, Beaudoin *et al.* 2004, Vino *et al.* 2004, 2005, Strachan *et al.* 2005, 2007, Beaudoin and Aider 2008) and numerical studies (Han 1989, Gillieron and Chometon 1999, Makowski and Kim 2000, Robinson 2001, Howard and Pourquie 2002, Kapadia *et al*. 2003a,b, Hinterberger *et al.* 2004, Bernard *et al.* 2005, Krajnovic and Davidson 2004a,b, 2005a,b,c, Fares 2006, Guilmineau 2008, Minguez *et al.* 2008). Due to the fact that it has been frequently used as a benchmark test case by researchers, Ahmed body has become a generic car-type bluff body with a slanted back. Furthermore, its simplified flow geometry allows easy comparisons between the results of experimental and numerical investigations (Lehmkuhl *et al.* 2012).

The flow around the Ahmed body is strongly influenced by angle of the rear slanted surface, which indicates that large portion of the aerodynamic drag is generated by development of three dimensional vortex separations from the rear slant surface (Guilmineau 2008). Three main flow phenomena can be seen in the complex downstream flow of the Ahmed body. These are recirculation bubble on the slanted surface, longitudinal vortices created on the side edges of the slanted surface and recirculation torus on the base of the body. In fact the pressure drag comes from rear part of the body and is related to the competition between these three strong coherent structures (Beaudoin and Aider 2008). Clearly, a more exact simulation of the wake flow and of the separation process is essential for the accuracy of drag predictions. In the experiments of Ahmed *et al*. (1984), a critical rear body slant angle $\varphi_c = 30^o$ was found at which the drag is maximum. This drag crisis is due to a drastic change in the flow structure. The flow evolves, when increasing the angle from a quasi-two-dimensional wake to a complex three-dimensional very dissipative structure. Beyond the critical angle, $\varphi_c = 30^o$, the wake becomes again quasi-two-dimensional (Guilmineau 2008).

Previous experimental studies conducted on investigation of the flow characteristics around the Ahmed body have largely employed intrusive and single point traditional measurement techniques, for example Pitot tubes, hotwire anemometry and laser Doppler anemometry techniques. These measurement techniques do not reveal instantaneous spatial structures of the flows. On the other hand, the Particle Image Velocimetry (PIV) technique, which is employed in this study, is capable of measuring the entire flow field simultaneously, without disturbing the flow. Furthermore, measurement of all unsteady flow features around the Ahmed body at the same time is extremely difficult in a tunnel by using any experimental techniques. For that purpose, computational fluid dynamics (CFD) is a powerful tool to understand the whole flow features around the Ahmed body. Han (1989) and Gillieron and Chometon (1999) conducted first significant numerical investigations of the flow around the Ahmed body by using Reynolds-averaged Navier-Stokes (RANS) solver. However, numerical studies conducted by RANS modelling have poor prediction of this flow. Large Eddy Simulation (LES) can be alternative to the conventional numerical methods. As a result, only a few attempts (Howard and Pourquie 2002, Hinterberger *et al.* 2004, Krajnovic and Davidson 2004a,b, 2005a,b,c, Minguez *et al.* 2008) have been made so far to apply the LES method to predict the flow features around the Ahmed body. Minguez *et al*. (2008) investigated the turbulent wake of the Ahmed body numerically for two different values of the Reynolds number, Re_H=8322 and 768000. They observed three recirculation zones, on the upper and lateral sides at the front part of the body, over the slant and behind the obstacle. They stated that the topology of the two flows was close, showing that the flow is not very sensitive to the Reynolds number, although the recirculation zones appeared at Re_H=8322 was larger and the lower

recirculation bubble in the downstream wake behind the obstacle was less pronounced. In the experimental study of Lienhart *et al*. (2000), conducted at Re_H=768000, no recirculation region at the front part of the Ahmed body was emphasized. On the other hand, in the numerical studies of Krajnovic and Davidson (2004a,b, 2005a,b) conducted at Re_H=200000, occurrence of recirculation bubbles on the upper and lateral sides at the front part of the body were reported. They stated that the simulated flow on the roof should be as similar as possible to those in the experiments at high Reynolds numbers. Thus, for the high Reynolds number if the roof flow does not separate at the leading edge, simulated flow at the low Reynolds number should not separate or should have as small separated regions as possible. However, they did not conclude that at the higher Reynolds number, Re_H=768000, such recirculation bubbles are still present (Minguez *et al*. 2008).

The main objective of this study is to investigate the flow characteristics around the Ahmed body, using both experimental and numerical methods. All these investigations provide a detailed quantitative description of highly complex and time dependent nature of the flow around the Ahmed body. Better understanding of the physical phenomena encountered in the wake flow of the Ahmed body is aimed. Investigations were conducted in two parts. In the first part, the LES method was used to resolve the flow structures around the body, numerically. In the second part, experimental measurements were completed. The PIV technique was used for the measurement of the instantaneous velocity fields around the body. Finally, quantitative results obtained with the aid of numerical calculations and experimental measurements were presented in terms of important turbulent flow properties and discussed in detail. Our numerical and experimental results were also compared with the results taken from literature.

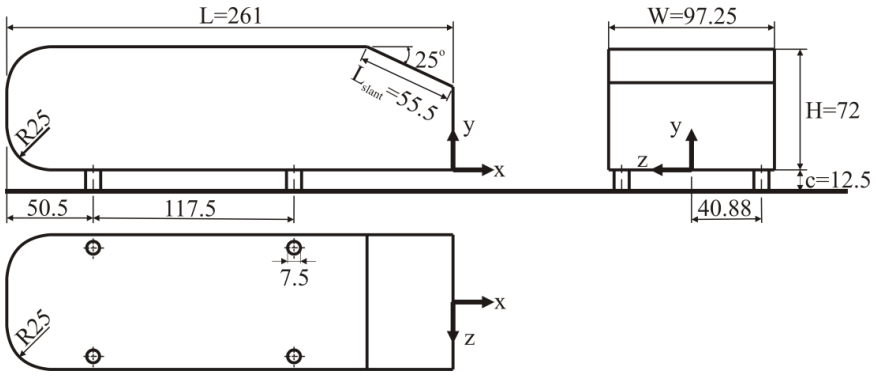

Fig. 1 ¼ scale Ahmed body geometry (Dimensions are in millimetre)

2. Experimental set-up and instrumentations

In the present study, ¼ scale Ahmed body having 25° slant angle geometry was employed as shown in Fig. 1. The model used in our PIV experiments was made up of a Plexiglas material.

Experiments were conducted in a recirculating, open surface water channel located in Cukurova University Fluid Mechanics Laboratory. The water channel test section had a width of 1000 mm, a depth of 750 mm, and a length of 8000 mm. Side and bottom walls of the test section were equipped with 15 mm thick Plexiglas for optical access. The flow was driven by a 15 kW

centrifugal pump having a variable speed controller. The maximum flow speed in the water channel is 250 mm/s. Before entering the test chamber, the flow passed through a settling reservoir, a honeycomb and a 2:1 contraction. The mean velocity was uniform and average turbulent intensity was less than 0.5% in the empty test section. Depth of water in the channel was maintained at H_w= 400 mm. Experiments were performed at a free stream velocity of U=207 mm/s which corresponded to the Reynolds number of Re_H=1.48x10^4 based on the model height. For the present experiments, a 2000 mm long ground plate mounted 100 mm above the bottom wall of the test section was used as a ground. The ground plate covered the cross section of the tunnel and had a rounded leading edge to avoid flow separation. Fig. 2 shows the location of the body in the water channel. The velocity fields were measured by Dantec PIV system which consisted of a dual-head Nd:YAG laser, a high resolution CCD camera, a synchronizer and optics. The measuring planes were illuminated by a thin and intense laser sheet by using a pair of double-pulsed Nd:YAG laser units. The time interval between pulses was 1.2 ms. The thickness of the laser sheet was approximately 2 mm. The time interval and the laser sheet thickness were selected such that the maximum amount of particle displacement in the interrogation window was obtained. The camera was equipped with a lens having focal length of 60 mm. The camera was placed at right angles to the light sheet. The resolution of the CCD camera was 1024x1024 pixels for image recording. The Nd:YAG laser and CCD camera were connected by using a Dantec FlowMap Processor synchronizer to control timing of the data acquisition. The flow was seeded with silver-coated spherical particles of 12 μm in average diameter. These particles are very close to being neutrally buoyant. The silver coated hollow particles were mixed in a container and poured into the water channel. Then, the water channel was run at maximum speed for a period of several minutes in order to ensure that particles were uniformly dispersed through the water. To determine the time-averaged mean flow structure, 350 instantaneous velocity fields were recorded successively for one series of image capturing with an acquisition frequency of 15Hz for each continuous run. Instantaneous velocity vector fields were generated using cross correlation technique between successive particle images. Dimensions of the interrogation area employed throughout the experiments were 32x32 pixels with 50% overlap providing 3844 (62x62) velocity vectors over the entire field of view plane. The overall field of view in the plane of the laser sheet was 140 mm×110 mm. According to the information given above, uncertainty in the mean velocity field and turbulent fluctuations were approximately 2% and 5% respectively. These instantaneous velocity fields were also time-averaged to obtain the corresponding time-averaged patterns of vorticity <ω> and streamline <ψ> topology.

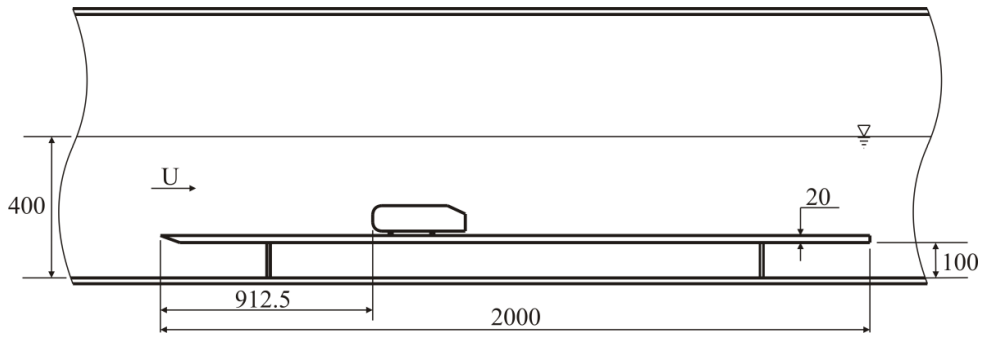

Fig. 2 Location of the Ahmed body in the water channel (Side view, dimensions are in Millimetre)

PIV measurements were performed in the vertical symmetry plane, z=0 and location of the laser sheet and view of the camera for measurement plane as well as the coordinate system are shown in Fig. 3. In the present study, coordinate systems x, y and z are the stream-wise, vertical and span-wise directions, respectively. The origin of this system was located in the symmetry plane and downstream bottom edge of the Ahmed body.

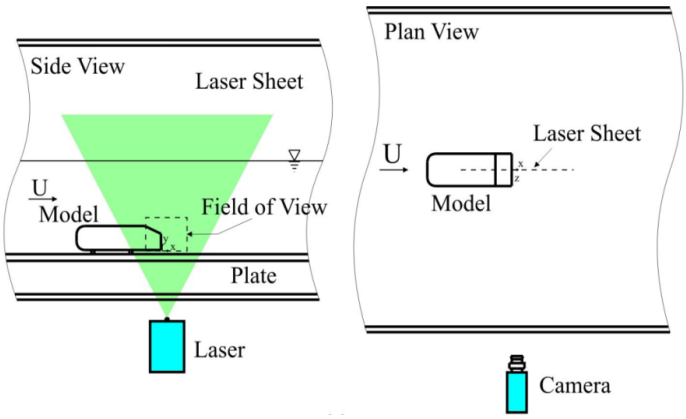

Fig. 3 Location of the laser sheet and view of the camera in the PIV measurements

In view of information available in the literature and previous work conducted in the present water tunnel, since the open gap between the Ahmed body and ground plate is 12.5 mm, it can be stated that the effect of boundary layer on the flow structures of the Ahmed body is negligible. For example, Wang *et al*. (2013) performed experimental work on the Ahmed body in a wind tunnel using a standard PIV system to visualize the flow around the model quantitatively with the Reynolds number, $Re_H \equiv 0.53x10^5$. They stated that the boundary layer disturbance thickness was 4 mm. Their estimation of boundary layer thickness was based on incoming velocity profile measured by the LDA at a location, 300 mm far from the leading edge of the plate. Aider *et al*. (2010) also performed experimental work on a 3-D bluff body similar to the Ahmed body using a PIV system. In their experiment, the boundary layer thickness was found to be 16 mm at a location 1200 mm downstream of the leading edge of the ground plate based on the Reynolds number, $2.4x10^6$. Gurlek *et al*. (2012) reported detailed experimental results of a bus model at the similar Reynolds number of the present work using a PIV system which were conducted in the same experimental set-up including raised ground plate and model location. They stated that the boundary layer on the ground plate was turbulent.

The predicted boundary layer thickness on the ground plate in the presence of the Ahmed body is 12 mm which is calculated numerically at a location 400 mm downstream of the leading edge of the ground plate or 122 mm upstream of the Ahmed body.

In conclusion, it is expected to have similar boundary layer thickness in the present work. Therefore, such a thin boundary layer thickness should have a negligibly small influence on the flow structure of the Ahmed body.

3. Numerical setup and computational geometry

The geometry of the computational domain is given in Fig. 4. The size of the computational domain in terms of the body height is 29H×5H×5H. All geometric quantities of the body, normalized with the body height, are as follows. The length of the body is L/H = 3.625, the length of the slant is L_{Slant}/H=0.771, the width of the body is W/H =1.347 and the radius of the front face is R/H =0.347. The body is located in the channel such that the upstream length between its front face and inlet of the channel is 7.25H and the downstream length between the rear face and outlet of the channel is 18.125H. The ground clearance between the body and floor is c/H=0.174.

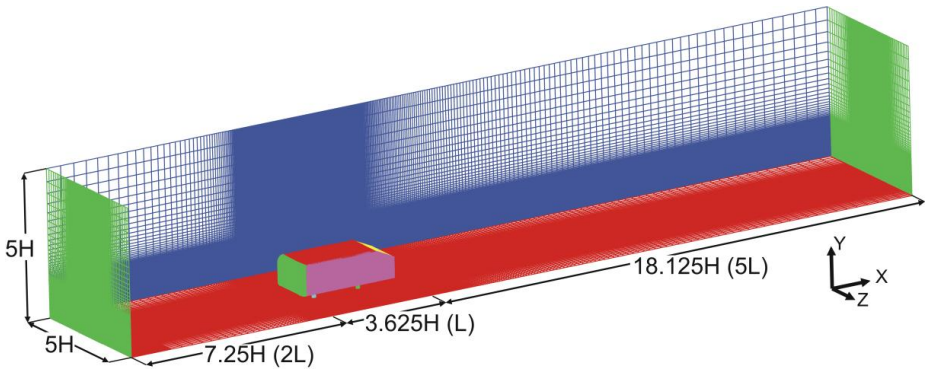

Fig. 4 Representation of the computational domain with the Ahmed body

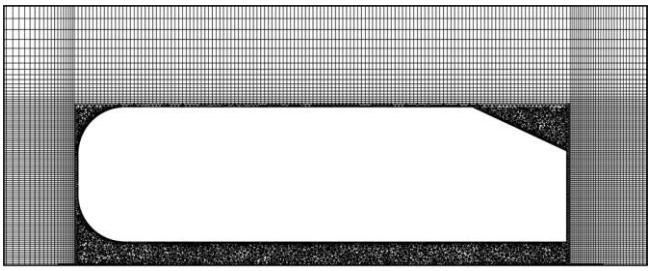

Fig. 5 View of the computational mesh in the vertical symmetry plane z=0

In the case of constructing mesh, our approach was to concentrate most of the grids in the region around the body. The Reynolds number value employed in our numerical study was corresponded to the same value of Reynolds number employed in our PIV measurements, which was Re_H =1.48x10^4. The computational domain was contained 8773309 cells. The close region around the Ahmed body contained 3709439 cells out of 8773309 cells.

Numerical accuracy was established by making LES simulations of three different computational meshes containing 1773952, 6797059 and 8773309 cells, respectively. Comparison of the averaged axial velocity component normalized with free stream velocity, <u>/U results of three different meshes is presented in Fig. 6.

3.1 Boundary and initial conditions

A uniform velocity profile constant in time, U=207 mm/s with a zero turbulence rate, was used as an inlet boundary condition. The level of turbulence at the inflow boundaries was assumed to be negligible. Therefore, fluctuating velocity components of the flow at the inlet boundaries were neglected and individual instantaneous velocity components were simply set equal to their mean velocity counterparts. At the outlet, diffusion fluxes for all flow variables in the exit direction were assumed to be zero. Surface of the body, bottom (ground) wall and lateral surfaces of the channel were treated as no-slip boundary condition. Upper surface of the channel was treated as slip surface using symmetry boundary condition. The initial conditions of the flow domain were computed from the previous solution of the steady RANS simulation.

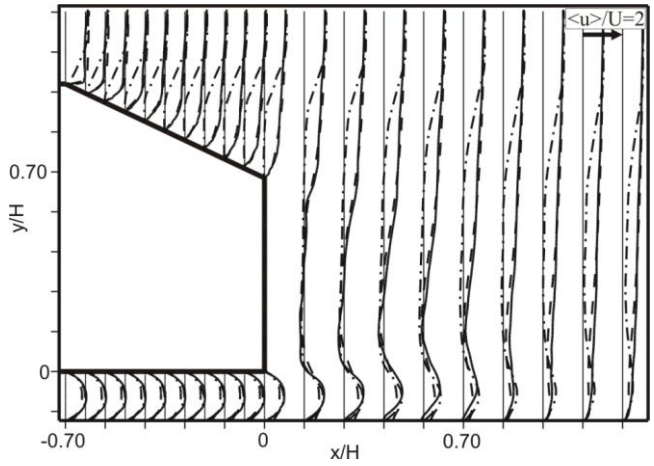

Fig. 6 Time-averaged normalized stream-wise velocity component <u>/U profiles in the vertical symmetry plane z=0 through the slanted surface and wake region of the Ahmed body. Fine mesh (solid curve), medium mesh (dashed curve) and coarse mesh (dashed-dotted curve)

3.2 Relevant length and time scales

In the numerical solution of the unsteady flow characteristics around the Ahmed body, it is necessary to set the time step Δt accordingly to model transient phenomena properly. The smallest timescale associated with turbulence can be approximated based on the Kolmogorov timescale $\Delta t_k \sim (H/U) Re_H^{-0.5}$, where Re_H represents the Reynolds number based on the characteristic velocity U and the characteristic length, H (Fares 2006). Therefore, the corresponding maximum time-step size in this study associated with the Kolmogorov timescale was 2.86×10^{-3} s. As a result, the time step-size employed in this study was 1×10^{-3} s. Besides, the maximum value of the cell Courant number throughout the simulation was approximately 3. In general, length of the simulation time used for averaging of the solution must be sufficiently long to produce mean solution that is not a function of time. Therefore, the averaging time, $t^* = tU/H$, in our simulation was 66.13 (23000 time

steps). This time interval is also equal to the time interval used in our PIV experiments and it is much larger than the one used in the studies of Krajnovic and Davidson (2004a,b).

For simulations of near-wall flows using the LES, another important parameter is the wall unit, $y^+ = u_\tau y/\nu$. In this study, computational grid had a resolution of y^+<6.6 in the wall normal direction. For the characterization of the mean flow field, relevant characteristic length scales associated with the flow over the Ahmed body are summarized in Table 1. In this table, λ_H and η_H represent the Taylor and the Kolmogorov length scales associated with the smallest turbulent scales of the flow, respectively. The maximum and the minimum cell distances normalized with the body height were 0.33 and $9.14\text{x}10^{-4}$, respectively.

Table 1 Selected relevant length scales of the simulation normalized with body height, *H*

L/H	*c/H*	*d/H*	λ_H/H	λ_H/H
3.625	0.174	0.104	$4.52\text{x}10^{-2}$	$8.93\text{x}10^{-4}$

3.3 Large eddy simulation

In the LES method, as it is known, large eddies are explicitly calculated (resolved) in a time-dependent simulation using the "filtered" Navier-Stokes equations. There are two major steps involved in the LES analysis: filtering and subgrid scale modelling. The filtering process effectively filters out eddies whose scales are smaller than the filter width used in the calculations. The resulting equations thus govern the dynamics of large eddies. Filtered incompressible continuity and Navier-Stokes equations used in this study are as follows.

$$\frac{\partial \bar{u}_i}{\partial x_i} = 0 \tag{1}$$

and

$$\frac{\partial \bar{u}_i}{\partial t} + \frac{\partial}{\partial x_j}\left(\bar{u}_i\,\bar{u}_j\right) = -\frac{1}{\rho}\frac{\partial \bar{p}}{\partial x_i} + \nu\frac{\partial^2 \bar{u}_i}{\partial x_j \partial x_j} - \frac{\partial \tau_{ij}}{\partial x_j} \tag{2}$$

where τ_{ij} is the subgrid-scale stress defined by

$$\tau_{ij} \equiv \rho\overline{u_i u_j} - \rho\bar{u}_i\bar{u}_j \tag{3}$$

The subgrid-scale stresses resulting from the filtering operation is unknown and modelled as follows

$$\tau_{ij} - \frac{1}{3}\tau_{kk}\delta_{ij} = -2\mu_t \bar{S}_{ij} \tag{4}$$

where μ_t is the subgrid-scale turbulent viscosity. The isotropic part of the subgrid-scale stresses τ_{kk} is not modelled, but added to the filtered static pressure term and $\bar{S}_{ij}$ is the rate-of-strain tensor for the resolved scale defined by

$$\overline{S_{ij}} \equiv \frac{1}{2}\left(\frac{\partial \bar{u}_i}{\partial x_j} + \frac{\partial \bar{u}_j}{\partial x_i}\right) \tag{5}$$

In the present study, the Smagorinsky-Lilly model was employed for the calculation of μ_t. In this model, the eddy viscosity is modelled by

$$\mu_t = \rho L_S^2 \left|\bar{S}\right| \tag{6}$$

where L_s is the mixing length for subgrid scales and $\left|\bar{S}\right| \equiv \sqrt{2\bar{S}_{ij}\bar{S}_{ij}}$. L_s is computed using

$$L_s = min(\kappa\, d\, C_s V^{1/3}) \tag{7}$$

where κ = 0.42, d is the distance to the closest wall, and V is the volume of the computational cell. The value of C_s=0.1 was used in the calculations.

3.4 Numerical implementation

Governing equations were discretized using finite volume method with the aid of Fluent package program. The numerical method employed to linearize and solve the discretized governing equations was rely on the pressure-based segregated algorithm. In this algorithm the momentum and continuity equations are sequentially solved wherein the constraint of mass conservation of the velocity field is achieved by solving a pressure correction equation. The pressure equation is derived from the continuity and the momentum equations in such a way that the velocity field, corrected by the pressure, satisfies the continuity. The SIMPLEC (Semi-Implicit Method for Pressure-Linked Equations-Consistent) algorithm was used to introduce pressure into the continuity equation. In simulations, a co-located scheme was used, whereby pressure and velocity are both stored at cell centres. PRESTO (PREssure STaggering Option) pressure interpolation scheme was used to calculate required face values of pressure from the cell values. Throughout the calculations, face values of scalars required for the convection terms in the discretized governing equation were interpolated from the discrete values of the scalar stored at the cell centres. This was accomplished by using a Bounded Central Differencing Scheme. The gradients of the flow variables at cell faces are computed by using node based Green-Gauss theorem, when discreatizing secondary diffusion terms and velocity derivatives in the flow conservation equations. The time derivative was discretized using the second-order discretization implicitly. A point implicit (Gauss-Seidel) linear equation solver was used in conjunction with an Algebraic Multigrid (AMG) method to solve the resultant scalar system of equations for the dependent variable in each cell.

4. Results and discussions

This section presents comparison of the mean and turbulent quantities of the LES and PIV results with some open literature data at different locations over the slanted surface and in the wake region of the Ahmed body. The LES and PIV results also provided time-averaged and instantaneous velocity vectors maps, vorticity contours, streamline topology and turbulence

characteristics of the flow. Flow features around the Ahmed body were well captured, such as separation and circulatory flows.

4.1 Time-averaged velocity field

Time-averaged velocity vectors maps <V>, the patterns of streamlines <ψ> and the corresponding vorticity contours <ω> along the Ahmed body in the vertical symmetry plane z=0 are presented in Fig. 7. In this figure, contours of positive and negative vorticity are indicated with solid and dashed lines, respectively.

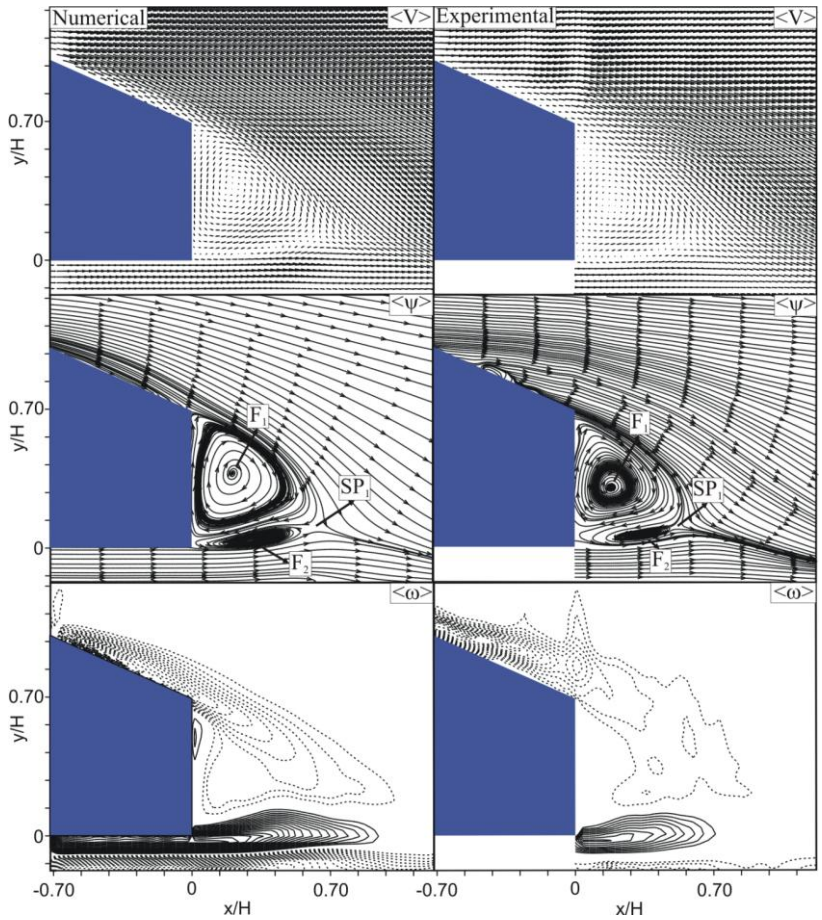

Fig. 7 Patterns of time-averaged velocity vectors maps <V>, streamlines <ψ> and vorticity contours <ω> in the vertical symmetry plane, z=0. Minimum and incremental values of vorticity are $<\omega_{min}>=\pm 4s^{-1}$ and $\Delta<\omega>=2s^{-1}$, respectively

The flow recirculation region formed downstream of the body is composed of two counter-rotating vortices. Regions of negative and positive vorticity contours are created with the upper-

body shear layer and the under-body shear layer, respectively. The bubble rotating in clockwise interacts with the upper region of the slanted surface of the body, while the lower bubble which rotates in the opposite direction covers the bottom surface. Size and central locations of bubbles indicated by the numerically calculated results agree well with the experimentally measured results. The under-body shear layer becomes smaller than the upper-body shear layer as a result of the ground effect. Jet-like flow emerging from the narrow gap between the bottom of the body and ground surface creates the base corner vortex. The time-averaged velocity vectors map, <V> and the corresponding patterns of streamline, $<\psi>$ clearly indicate the locations of the saddle point (SP_1) and focuses (F_1 and F_2) which are located in the near wake region ($0<x/H<0.70$) downstream of the body. Comparisons of the numerically calculated and experimentally measured locations of these critical points are presented in Table 2. In this table, distances are normalized with body height, *H*. Analysing the table, it can be seen that the LES calculations well predict the locations of all critical points in the near wake region with differences less than 11% from the results of PIV measurements. The maximum difference in the stream-wise direction between the calculated and measured locations of the critical points occurs for the location of saddle points (SP_1) with a value of 11%. In the same way, the maximum difference in the vertical direction occurs for the locations of the focus points (F_1) with a value of 8%.

Although there is good agreement between the flow characteristics revealed from the numerical and experimental investigations with the results of previous literature in the wake region downstream of the Ahmed body, the differences were found on the slanted surface of the body. Previous studies (Ahmed *et al.* 1984, Lienhart *et al.* 2000, Krajnovic and Davidson 2005a,b, Minguez *et al.* 2008) have shown that the flow separates at the top edge of the rear slant, reattaches roughly half-way down the slant and thereafter remains attached due to the presence of strong side-edge vortices. In this study, very small recirculation region in the vertical symmetry plane z=0 through the slanted surface of the body is observed. This recirculation region is more distinctive in the experimental results than the numerical results. The flow separates at a point nearly half of the slanted surface from the beginning. Beyond this region, the flow then reattaches to the slanted surface of the body.

Table 2 Comparison of the numerically calculated and experimentally measured locations of the critical points with the corresponding results of Krajnovic and Davidson (2005a) in the vertical symmetry plane z=0 through the near wake region downstream of the Ahmed body

	Saddle Point (SP_1)		Focus Point 1 (F_1)		Focus Point 2 (F_2)	
	Num.	Exp.	Num.	Exp.	Num.	Exp.
X (*x/H*)	0.60	0.49	0.21	0.18	0.36	0.35
Y (*y/H*)	0.10	0.10	0.38	0.30	0.05	0.06

4.2 Time-averaged velocity profiles

In Figs. 8 and 9, time-averaged normalized stream-wise, <u>/*U* and vertical, <v>/*U* velocity profiles obtained by using LES calculations and PIV measurements in the vertical symmetry plane *z*=0 through the slanted surface and wake region downstream of the Ahmed body are presented. They are also compared, in the same figures, with the experimental data of Lienhart *et al.* (2000) at the corresponding locations on the slanted surface and in the wake region downstream of the

Ahmed body. In all figures of velocity profiles, the velocity profiles are presented at positions between x/H=-0.70 and 1.25, where the length intervals between two velocity profiles are $\Delta x/H$=0.069 and 0.139 on the slanted surface and through the wake region downstream of the body, respectively. Stream-wise and vertical velocity profiles presented by the results of the LES calculations are in good agreement with the experimental data at almost all positions on the slanted surface and in the wake region as shown in Figs. 8 and 9. In general, rapid changes in the vertical velocity profiles occur on the slanted surface and along the upper and under body shear layers. These velocity profiles reveal that there is an intense shear throughout the velocity field.

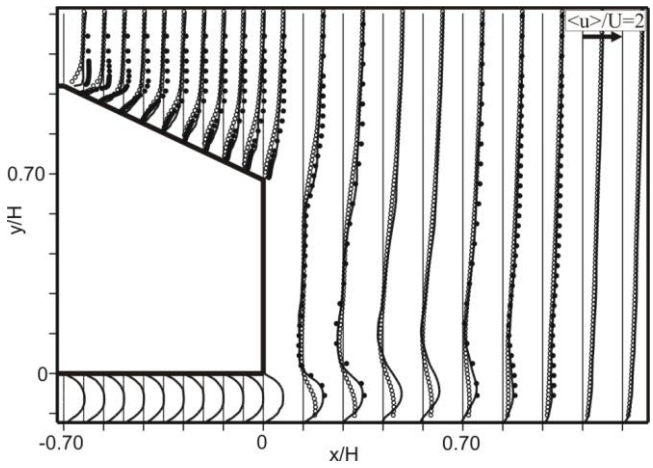

Fig. 8 Time-averaged normalized stream-wise velocity component <u>/U profiles in the vertical symmetry plane z=0 through the slanted surface and wake region of the Ahmed body. LES results (solid curve), PIV results (empty circles) and results of Lienhart *et al.* (2000) (filled circles)

Stream-wise velocity results of Lienhart *et al.* (2000) presented negative values between x/H=-0.625 and -0.347 which means that flow separates just after the beginning of the slanted surface and re-attaches almost at the half-point of the slanted surface. On the other hand, stream-wise velocity results of the PIV measurements on the slanted surface show negative values only at the location of x/H=-0.347 and stream-wise velocity results of the LES calculations on the slanted surface show negative values between x/H=-0.556 and -0.0694. This means that the location of the separation point of the flow on the slanted surface is somewhat delayed at Re_H=1.48x10^4 comparing to high Reynolds numbers in the vertical symmetry plane z=0. PIV measurements and LES calculations can compute a small separation bubble on the slanted surface between the half-point and end-point of the slanted surface. The flow downstream of the body is reversed causing a negative velocity distributions between locations of x/H=0 and 0.556. The maximum reversed velocities in the recirculatory flow region are approximately -0.193, -0.280, -0.337 times the free-stream velocity, U according to the results of the PIV measurements, LES calculations and Lienhart *et al.* (2000) measurements, respectively. It is noteworthy that the locations of the maximum reversed velocity are approximately at the same point in both experimental and numerical results, which are about x/H=0.278 and y/H=0.113 in the stream-wise and vertical

directions, respectively. In the first measuring plane at the position of *x/H*=0.139, stream-wise velocity components take negative values between *y/H*=0.0126 and 0.256, 0.0150 and 0.378, 0.0278 and 0.271 as indicated by the results of the PIV measurements, LES calculations and Lienhart *et al.* (2000) measurements, respectively. Stream-wise velocity components also take negative values at three locations such as *x/H*=0.278, 0.417 and 0.556 with decreasing amount. Due to the jet flow occurring between the ground and the bottom surface of the body, the value of stream-wise velocity increases in the lower part of the wake region. The jet flow emanating from the narrow gap between the ground board and the bottom surface of the body travels towards the mid-section of the wake and later interacts with the flow coming from the slanted surface of the body. As a result of this interaction, a negative velocity region also called as near wake region occurs downstream of the body. Besides, the rate of increase in the stream-wise velocity across the shear layer at the upper part of the body is due to the entrainment between the wake and core flow regions. Since the fifth measuring section in the wake region, *x/H*=0.70 correspond to just after the saddle point, stream-wise velocity distribution profiles after this location do not indicate any negative velocity value.

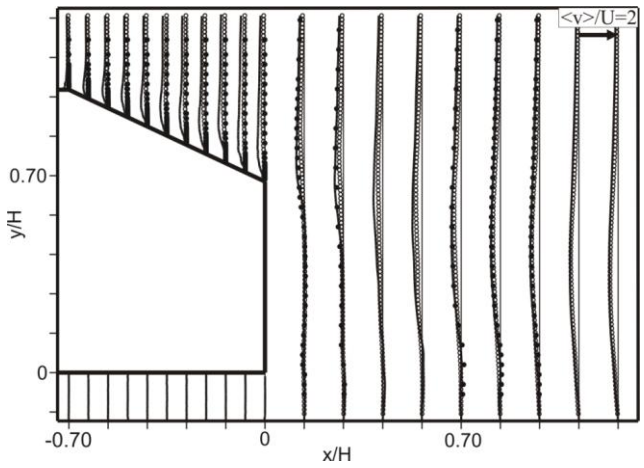

Fig. 9 Time-averaged normalized vertical velocity component <v>/*U* profiles in the vertical symmetry plane *z*=0 through the slanted surface and wake region of the Ahmed body. LES results (solid curve), PIV results (empty circles) and results of Lienhart *et al.* (2000) (filled circles)

In Fig. 9, positive and negative vertical velocity, <v>/*U* results in the near wake indicates upsweep and down-sweep flow, respectively. The maximum upsweep velocities are 0.0428, 0.111, 0.138 times the free stream velocity, *U* according to the results of the PIV measurements, LES calculations and Lienhart *et al.* (2000) measurements, respectively. Locations of the maximum upsweep velocity are nearly at the same point in both PIV and LES results which are approximately *x/H*=0.417 and *y/H*=-0.0428. Furthermore, the maximum down-sweep velocities are -0.413,-0.492, -0.478 times the free stream velocity, *U* as revealed by the results of the PIV measurements, LES calculations and Lienhart *et al.* (2000) measurements, respectively. Locations of the maximum down-sweep velocities in the stream-wise direction are at position of *x/H*=0.70

for both LES results and results of Lienhart *et al.* (2000) and *x/H*=1.11 for the PIV results. Locations of the maximum down-sweep velocities in the vertical direction are *y/H*=0.414, 0.490 and 0.583 as indicated by the PIV measurements, LES calculations and Lienhart *et al.* (2000) measurements, respectively.

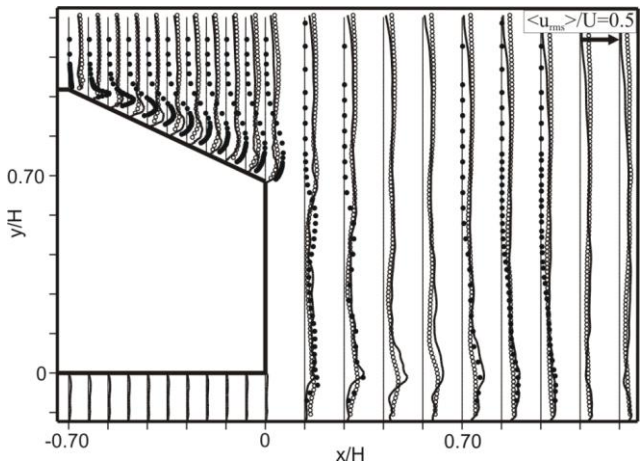

Fig. 10 Time-averaged normalized root mean square of stream-wise velocity component $\langle u_{rms} \rangle / U$ profiles in the symmetry plane z=0 through the slanted surface and wake region of the Ahmed body. LES results (solid curve), PIV results (empty circles) and results of Lienhart et al. (2000) (filled circles).

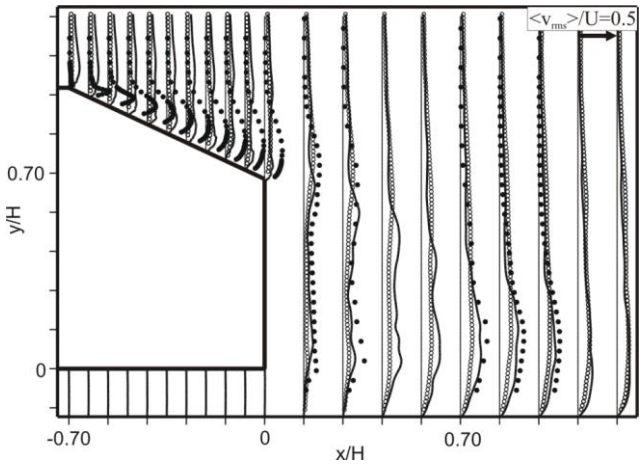

Fig. 11 Time-averaged normalized root mean square of vertical velocity component $\langle v_{rms} \rangle / U$ profiles in the symmetry plane z=0 through the slanted surface and wake region of the Ahmed body. LES results (solid curve), PIV results (empty circles) and results of Lienhart et al. (2000) (filled circles).

Figs. 10, 11 and 12 present profiles of the time-averaged root mean square of the stream-wise $\langle u_{rms} \rangle / U$ and vertical $\langle v_{rms} \rangle / U$ velocity components normalized by the free stream velocity U and time-averaged Reynolds stress correlation $\langle u'v' \rangle / U^2$ normalized by square of the free stream velocity U^2 in the vertical symmetry plane z=0, respectively. Locations of the peak values of these turbulence quantities hold places along the upper-body and under-body shear layers and their magnitudes are higher in the under-body shear layer than that of in the upper-body shear layer.
Additionally, the peak values and the locations of $\langle u_{rms} \rangle / U$, $\langle v_{rms} \rangle / U$ and $\langle u'v' \rangle / U^2$ in the upper-body and under-body shear layers provided by the results of the PIV measurements, LES calculations and Lienhart *et al.* (2000) measurements are given in Table 3. According to this table, the maximum values of the turbulence quantities found in the upper-body and under-body shear layer are aligned with the trailing edge of the slanted surface and the bottom end of the body, respectively, in the vertical direction. The results presented in Table 3 also show that while the maximum values of turbulence quantities found in the upper-body shear layer are formed just after the body, their maximum values found in the under-body shear layer are formed around the end of the near wake in the stream-wise direction. On the other hand, there are some differences between the present turbulence quantities results and the corresponding results of Lienhart *et al.* (2000) on the slanted surface of the Ahmed body. The previous results show that the peak turbulence quantities values are found at downstream of the leading edge of the slanted surface where the flow separates. However, in the present LES calculations and PIV measurements the location of the peak turbulence quantities values are appeared at the location somewhat downstream compared to the results of Lienhart *et al.* (2000). This situation is also observed in the study of Minguez *et al.* (2008) and they indicated that it is probably due to the upstream flow where the recirculation bubble in the flow separation region interacts with the shear layer shedding from the roof.

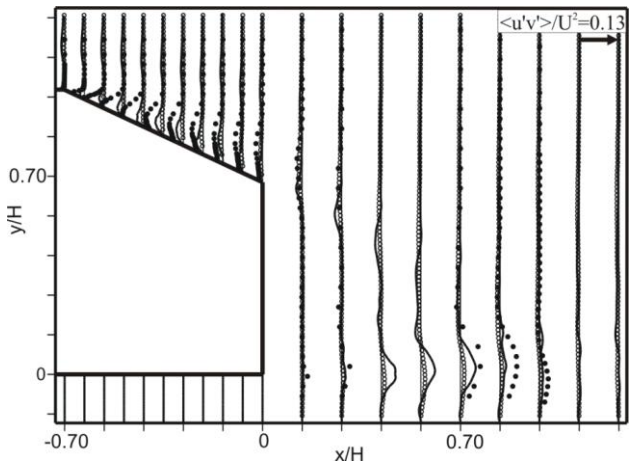

Fig. 12 Time-averaged normalized Reynolds stress correlation $\langle u'v' \rangle / U^2$ profiles in the symmetry plane z=0 through the slanted surface and wake region of the Ahmed body. LES results (solid curve), PIV results (empty circles) and results of Lienhart et al. (2000) (filled circles)

4.3. Instantaneous velocity field

Numerically and experimentally obtained instantaneous flow structures in the vertical symmetry plane z=0 through the wake region downstream of the Ahmed body are presented in

Table 3 Peak values and their locations of $<u_{rms}>/U$, $<v_{rms}>/U$, $<u'v'>/U^2$ in the vertical symmetry plane z=0 through the upper-body and under-body shear layers in the wake region downstream of the Ahmed body

		Upper-body Shear Layer			Under-body Shear Layer		
			Locations of Peak Value			Locations of Peak Value	
		Peak Value	In the Stream-wise Direction (x/H)	In the Vertical Direction (y/H)	Peak Value	In the Stream-wise Direction (x/H)	In the Vertical Direction (y/H)
$<u_{rms}>/U$	LES Results	0.159	0.139	0.658	0.306	0.417	-0.0130
	PIV Results	0.156	0.139	0.715	0.194	0.556	-0.0160
	Lienhart *et al*. (2000)	0.178	0.139	0.757	0.315	0.480	-0.0111
$<v_{rms}>/U$	LES Results	0.221	0.417	0.462	0.262	0.70	0.0569
	PIV Results	0.134	0.417	0.614	0.152	0.70	0.113
	Lienhart *et al*. (2000)	0.200	0.139	0.722	0.339	0.70	0.0972
$<u'v'>/U^2$	LES Results	-0.0223	0.278	0.560	0.0479	0.70	0.0289
	PIV Results	-0.0106	0.139	0.729	0.0133	0.556	-0.016
	Lienhart *et al*. (2000)	-0.0163	0.139	0.757	0.0626	0.70	0.0278

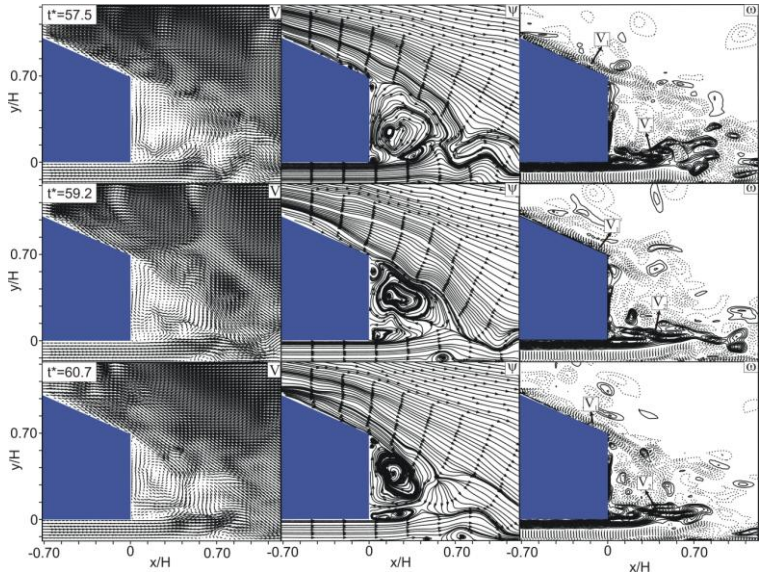

Fig. 13 Patterns of numerically obtained instantaneous velocity vectors maps V, streamlines ψ and vorticity contours ω in the vertical symmetry plane z=0 for instants of t^*=57.5, 59.2 and 60.7. Minimum and incremental values of vorticity are $\omega_{min}=\pm 5s^{-1}$ and $\Delta\omega=5s^{-1}$, respectively

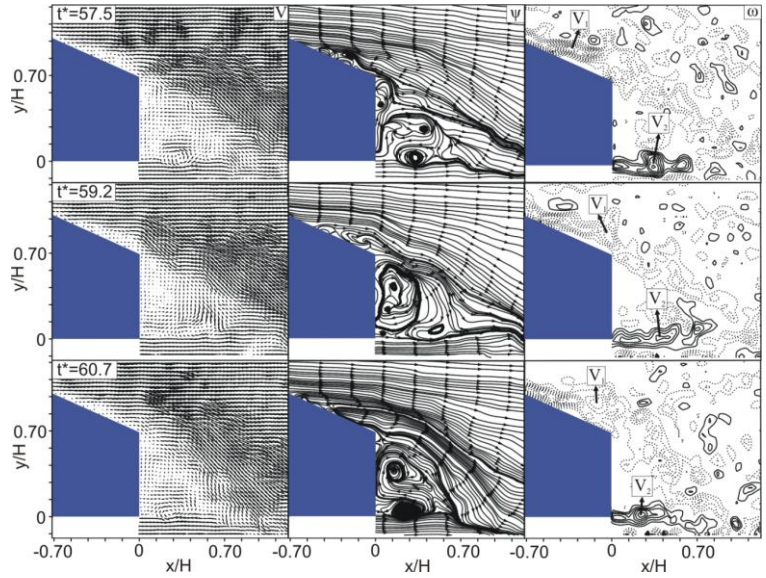

Fig. 14 Patterns of experimentally obtained instantaneous velocity vectors maps V, streamlines ψ and vorticity contours ω in the vertical symmetry plane z=0 for instants of t^*=57.5, 59.2 and 60.7. Minimum and incremental values of vorticity are $\omega_{min}=\pm 5s^{-1}$ and $\Delta\omega=5s^{-1}$, respectively

Figs. 13 and 14 respectively for instants of t^*=57.5, 59.2 and 60.7. Here t^* is dimensionless time defined as $t^*=tU/H$. Distributions of the flow parameters in these figures indicate that swirling patterns of velocity vectors take place on the slanted surface and in the wake region of the body. Furthermore, well defined large-scale swirling patterns of the velocity vectors are evident at the bottom edge of the vertical base of the body. Shear layers emanating from the upper-body and under-body surfaces cause complex flow field consisting of a number of vortices that move randomly in time and space. Two main vortices are developed in the wake of the body. One comes from the lower side of the rear wall of the body and the other one comes from the slanted surface of the body. As clearly shown in Figs. 13 and 14 that positive vortex V_2 induced in the under-body shear layer grows in size, elongates and loses its strength. As soon as vortex V_2 enlarges in size, it moves upward and downward in the vertical direction and attenuates further downstream.

Highly turbulent flow character of the flow around the Ahmed body is also confirmed by conducting spectral analysis of time variations of the experimentally and numerically obtained stream-wise and vertical velocity components at different points in the flow. The spectra of the stream-wise and vertical velocity fluctuations obtained by applying FFT analysis at four selected points in the vertical symmetry plane are presented in Fig. 15. The locations of these selected points are taken as point 1 which is on the slanted surface at x/H=-0.23, y/H=0.83; point 2 which is in the inner part of the upper shear layer at x/H=0.26, y/H=0.60; point 3 which is in the outer part of the upper shear layer at x/H=0.55, y/H=0.60 and point 4 which is in the lower shear layer at x/H=0.61, y/H=-0.03 in the wake region. The dominant frequency in the experimental study was found as f=0.88 for both stream-wise and vertical velocity fluctuations at the fourth point in the lower shear layer which leads to the Strouhal number of $St=fH/U$=0.31 (based on the model height H and the free steam velocity U). In the numerical study, the dominant frequency was found as f=1.35 for stream-wise velocity fluctuations which leads to the Strouhal number of $St=fH/U$=0.47

at the fourth point as obtained in the experiments. These results correspond with the numerical result of Minguez *et al.* (2008), which is *St*=0.42, for the same flow geometry at $Re_H=7.68x10^5$. On the other hand, no dominant frequency value was found as indicated by the numerical results of the vertical velocity fluctuations for the selected points in the wake region.

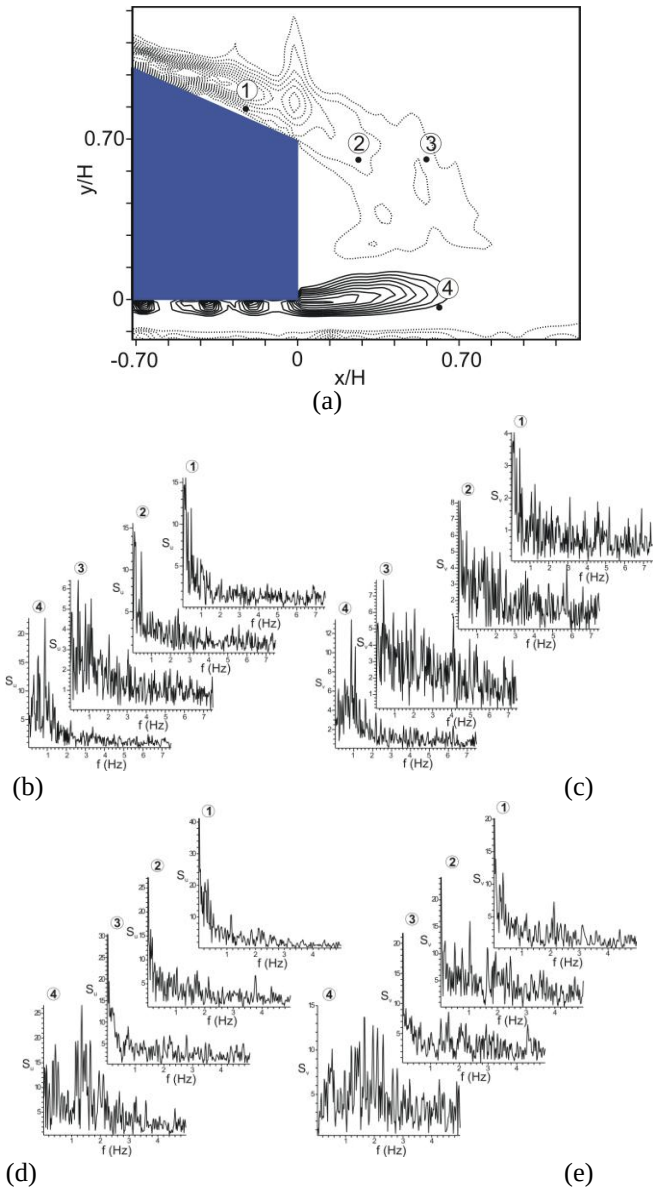

Fig. 15 The spectrum of experimentally obtained stream-wise u (b) and vertical v (c) velocity component fluctuations and the spectrum of numerically obtained stream-wise u (d) and vertical v (e) velocity component fluctuations for selected points in the vertical symmetry plane *z*=0 shown in (a)

5. Conclusions

The present study aims to investigate characteristics of the flow around the ground vehicles with the aid of Ahmed body using both experimental and numerical methods. Flow structures such as critical points and recirculation zone downstream of the body were well captured. Size and centre locations of the critical points obtained by using the LES calculations agree well with the PIV measurements. Although there is good agreement between the flow characteristics revealed from the numerical and experimental investigations with the results of previous literature in the wake region downstream of the Ahmed body, the differences were found on the slanted surface of the body. Very small recirculation region on the slanted surface of the body was observed. The spectra of experimentally obtained stream-wise and vertical velocity fluctuations show dominant frequency of f=0.88, at the location of x/H=0.61 and y/H=-0.03, in the lower shear layer downstream of the body which corresponds to the Strouhal number of St=0.31. Moreover, only the spectra of numerically obtained stream-wise velocity fluctuations shows dominant frequency of f=1.35, at the same location which corresponds to the Strouhal number of St=0.47. These results are consistent with the numerical result of Minguez *et al.* (2008), which is St=0.42, for the same flow geometry at $Re_H=7.68x10^5$.

Acknowledgements

The authors would like to acknowledge the financial support of the office of Scientific Research Projects of Cukurova University for funding under contract no: AAP20025

References

Ahmed, S.R., Ramm, G. and Faltin, G. (1984), *Some salient features of the time-averaged ground vehicle wake*, SAE Technical Paper.

Aider J.L., Beaudoin J.F. and Wesfreid J.E. (2010), "Drag and lift reduction of a 3D bluff-body using active vortex generators", *Exp. Fluids*, **48**(5), 771-789.

Barlow, J., Guterres, R., Ranzenbach, R. and Williams, J. (1999), *Wake structures of rectangular bodies with radiused edges near a plane surface*, SAE Paper.

Barlow, J.B., Guterres, R., and Ranzenbach, R. (1999), Rectangular bodies with radiused edges in ground effect, AIAA Paper No. 99-3153.

Beaudoin, J.F. and Aider, J.L. (2008), "Drag and lift reduction of a 3D bluff body using flaps", *Exp. Fluids*, **44**(4), 491-501.

Beaudoin, J.F., Cadot, O., Aider, J.L., Gosse, K., Paranthoen, P., Hamelin, B., Tissier, M., Allano, D., Mutabazi, I., Gonzales, M. and Wesfreid, J.E. (2004), "Cavitation as a complementary tool for automotive aerodynamics", *Exp. Fluids*, **37**(5), 763-768.

Bernard, P.S., Collins, P. and Potts, M. (2005), *Vortex method simulation of ground vehicle aerodynamics*, SAE Technical papers.

Cooper, K. R. (1985), *The effect of front-edge rounding and rear edge shaping on the aerodynamic drag of bluff vehicles in ground proximity*, SAE Paper.

Fares, E. (2006), "Unsteady flow simulation of the Ahmed reference body using a lattice boltzmann approach", *Comput. Fluids*, **35**(8-9), 940-950.

Gilliéron, P. and Chometon, F. (1999), "Modelling of stationary three-dimensional separated air flows around an Ahmed reference model", *Proceedings of the 3rd International Workshop on Vortex ESAIM*.

Guilmineau, E. (2008), "Computational study of flow around a simplified car body", *J. Wind Eng. Ind. Aerod.*, **96**(6-7), 1207-1217.
Gurlek, C., Sahin, B., Ozalp, C. and Akilli, H. (2008), "Flow structures around a three-dimensional rectangular body with ground effect", *Wind Struct*., **11**(5), 345-359.
Gurlek C., Sahin B. and Ozkan G.M. (2012), "PIV studies around a bus model", *Exp. Therm. Fluid Sci*., **38**, 115-126.
Han, T. (1989), "Computational analysis of three-dimensional turbulent flow around a bluff body in ground proximity", *AIAA J.*, **27(9)**, 1213-1219.
Hinterberger, C., Garcia-Villalba, M. and Rodi W. (2004), *Large eddy simulation of flow around the Ahmed body*, The aerodynamics of heavy vehicles: trucks, buses and trains, Lecture Notes in Applied and Computational Mechanics, Springer, Berlin.
Howard, R.J.A. and Pourquie, M. (2002), "Large eddy simulation of an Ahmed reference model", *J. Turbul*., **3**.
Hucho, W.H. and Sovran, G. (1993), "Aerodynamics of road vehicles", *Annu. Rev. Fluid Mech.*, **25**, 485-537.
Kapadia, S., Roy, S., Vallero, M., Wurtzler, K. and Forsythe, J. (2003), "Detached-eddy simulation over a reference Ahmed car model", *Proceedings of the Direct and Large-Eddy Simulation-V*, Garching, Germany, 27-29 August.
Kapadia, S., Roy, S. and Wurtzler, K. (2003), "Detached eddy simulation over a reference Ahmed car model", *Proceedings of the 41st Aerospace Sciences Meeting and Exhibit*, Reno, Nevada, 6-9 January.
Krajnovic, S. and Davidson, L. (2004), "Large eddy simulation of the flow around an Ahmed body", *Proceedings of the HTFED04, ASME Heat Transfer/Fluids Engineering Summer Conference*, Charlotte, North Carolina, USA.
Krajnovic, S. and Davidson, L. (2004), "Large-eddy simulation of the flow around simplified car model", *Proceedings of the SAE World Congress*, SAE Paper No. 2004-01-0227, Detroit, USA.
Krajnovic, S. and Davidson, L. (2005), "Flow around a simplified car, Part 1: large eddy simulation", *J. Fluid. Eng. – T. ASME*, **127**(5), 907-918.
Krajnovic, S. and Davidson, L. (2005), "Flow around a simplified car, Part 2: understanding the flow", *J. Fluid. Eng. – T. ASME*, **127**(5), 919-928.
Krajnovic, S. and Davidson, L. (2005), "Influence of floor motions in wind tunnels on the aerodynamics of road vehicles", *J. Wind Eng. Ind. Aerod*., **93**, 677-696.
Lehmkuhl, O., Borrell, R., Rodriguez, I., Perez-Segarra, C.D. and Oliva, A. (2012), "Assessment of the symmetry-preserving regularization model on complex flows using unstructured grids", *Comput. Fluids*, **60**, 108-116.
Lienhart, H., Stoots, C. and Becker, S. (2000), "Flow and turbulence structures in the wake of a simplified car model (Ahmed model)", *Proceedings of the DGLR Fach. Symp. der AG STAB DGLR Fach. Symp. der AG STAB*, Stuttgart University.
Makowski, F.T. and Kim, S.E. (2000), *Advances in external-aero simulation of ground vehicles using the steady RANS equations*, SAE Technical Paper Series, World Congress Detroit, Michigan, 6-9 March.
Minguez, M., Pasquetti, R. and Serre, E. (2008), "High-order large-eddy simulation of flow over the "Ahmed body" car model", *Phys. Fluids*, **20**(9), 095101.
Robinson, C.M.E. (2001), *Advanced CFD modelling of road-vehicle aerodynamics*, PhD thesis, Institute of Science and Technology of University of Manchester.
Sharma, R., Chadwick, D. and Haines, J. (2008), "Aerodynamics of an intercity bus", *Wind Struct*., **11**(4), 257-273.
Spohn, A. and Gillieron, P. (2002), "Flow separations generated by a simplified geometry of an automotive vehicle", *Proceedings of the IUTAM Symposium: Unsteady Separated Flows*, Toulouse, France, April 8-12.
Strachan, R., Knowles, K. and Lawson, N. (2005), "Comparisons between CFD and experimental results for a simplified car model in wall proximity", *Proceedings of the Integrating CFD and Experiments in Aerodynamics*, 5-6 September.

Strachan, R., Knowles, K. and Lawson, N. (2007), "The vortex structure behind an Ahmed reference model in the presence of a moving ground plane", *Exp. Fluids*, **42**(5), 659-669.
Vino, G., Watkins, S., Mousley, P., Watmuff, J. and Prasad, S. (2004), "The unsteady near-wake of a simplified passenger car", *Proceedings of the 15th Australasian Fluid Mechanics Conference*, Sydney, Australia.
Vino, G., Watkins, S., Mousley, P., Watmuff, J. and Prasad, S. (2005), "Flow structures in the near-wake of the Ahmed model", *J. Fluid. Struct.*, **20**(5), 673-695.
Wang X.W., Zhou Y., Pin Y.F. and Chan T.L. (2013), "Turbulent near wake of an Ahmed vehicle model", *Exp. Fluids*, **54**, 1490-1509.

CC